PNAS RESEARCH ARTICLE | APPLIED PHYSICAL SCIENCES

Thermodynamics of calcium binding to heparin: Implications of solvation and water structuring for polysaccharide biofunctions

Brenna M. Knight[a,b], Connor M. B. Gallagher[a,b], Michael D. Schulz[a,b], Kevin J. Edgar[b,c], Caylyn D. McNaul[d], Christina A. McCutchin[a,b], and Patricia M. Dove[b,e,f,1]

Affiliations are included on p. 9.

Contributed by Patricia M. Dove; received February 26, 2025; accepted July 24, 2025; reviewed by Bruno M. Moerschbacher, Jia Niu, and Jeffrey D. Rimer

Heparan sulfates are found in all animal tissues and have essential roles in living systems. This family of biomacromolecules modulates binding to calcium ions (Ca^{2+}) in low free energy reactions that influence biochemical processes from cell signaling and anticoagulant efficacy to biomineralization. Despite their ubiquity, the thermodynamic basis for how heparans and similarly functionalized biomolecules regulate Ca^{2+} interactions is not yet established. Using heparosan (Control) and heparins with different positions of sulfate groups, we quantify how SO_3^- and COO^- content and SO_3^- position modulate Ca^{2+} binding by isothermal titration calorimetry. The free energy of all heparin-Ca^{2+} interactions (ΔG_{rxn}) is dominated by entropic contributions due to favorable water release from polar, hydrophilic groups. Heparin with both sulfate esters (*O*-SO_3^-) and sulfamides (*N*-SO_3^-) has the strongest binding to Ca^{2+} compared to heparosan and to heparin with only *O*-SO_3^- groups (~3X). By linking Ca^{2+} binding thermodynamics to measurements of the interfacial energy for calcite ($CaCO_3$) crystallization onto polysaccharides, we show molecule-specific differences in nucleation rate can be explained by differences in water structuring during Ca^{2+} interactions. A large entropic term ($-T\Delta S_{rxn}$) upon Ca^{2+}–polysaccharide binding correlates with high interfacial energy to $CaCO_3$ nucleation. Combining our measurements with literature values indicates many Ca^{2+}–polysaccharide interactions have a shared thermodynamic signature. The resulting enthalpy–entropy compensation relationship suggests these interactions are generally dominated by water restructuring involving few conformational changes, distinct from Ca^{2+}–protein binding. Our findings quantify the thermodynamic origins of heparin-specific interactions with Ca^{2+} and demonstrate the contributions of solvation and functional group position during biomacromolecule-mediated ion regulation.

entropy | biomaterial | biomineralization | calcite | calorimetry

Significance

Calcium ion (Ca^{2+}) interactions with macromolecules regulate many biological functions. This study quantifies the strength of Ca^{2+} binding to three heparin family molecules and shows the binding is an entropy-dominated reaction through release of water molecules to increase disorder. Water rearrangement may also explain polysaccharide-specific rates of calcite ($CaCO_3$) nucleation. Combining our data with published Ca^{2+} binding measurements indicates changes in water structuring also occur for many other biomacromolecules. However, polysaccharides and proteins present distinct enthalpy–entropy compensation relationships during interactions with Ca^{2+}, suggesting a thermodynamic basis for how macromolecules can regulate cation activity in the low free energy reactions of biological systems. Viewing biomacromolecule–Ca^{2+} binding through the lens of solvation provides mechanistic insight for biomaterial innovations.

In living systems, calcium ion (Ca^{2+}) interactions with proteins, polysaccharides, and/or nucleic acids are low free energy (ΔG_{rxn}) reactions that serve crucial functions such as regulating enzymatic activity, cell signaling, and providing structural integrity to tissues (1–4). Studies of Ca^{2+}-binding proteins show that biomacromolecule affinity for Ca^{2+} must lie within a biologically functional window of ΔG_{rxn} that is large enough to present some stability but small enough to allow for reactivity without kinetic trapping (5, 6). Among the polysaccharides, the glycosaminoglycan (GAG) macromolecules have critical roles in the extracellular matrix and cellular communication that involve interactions with Ca^{2+}(7–9), though the free energies of these interactions are not well established.

Biomolecules of the heparan sulfate group are important members of the GAG family and are near-ubiquitous in the cells of all major branches of animals (Fig. 1) (10). From cnidarians and arthropods to echinoderms and mammals, the primary structural features of these molecules, including the main disaccharide unit (a hexuronic acid and hexosamine that contain sulfate esters), have been conserved throughout evolution (11). However, differences in the number [as indicated by degree of substitution (DS)] and position of sulfate groups within the disaccharide may reflect specialized or species-specific functions. Heparan sulfate molecules begin as heparosan (Fig. 2*A*), with a consistent repeat unit of glucuronic acid (GlcA) and acetyl glucosamine (GlcNAc) and thus contain carboxylates as their only acidic moiety. Heparosan can be subsequently "decorated" with sulfate (SO_3^-) groups at one or more *O*-positions (Fig. 2*B*) and/or at the C2N-position (Fig. 2*C*) to yield heparin. Some degree of epimerization at C5 of the hexuronic acid monosaccharides [from GlcA to iduronic acid (IdoA)] and loss of molecular weight also occur. Heparin that is both *N*- and *O*-sulfated (Fig. 2*C*) has particular importance to mammalian systems and biomedicine due to its

Reviewers: B.M.M., University of Münster; J.N., Boston College; and J.D.R., University of Houston.

The authors declare no competing interest.

[1]To whom correspondence may be addressed. Email: pdove@vt.edu.

This article contains supporting information online at https://www.pnas.org/lookup/suppl/doi:10.1073/pnas.2504348122/-/DCSupplemental.

Published August 26, 2025.

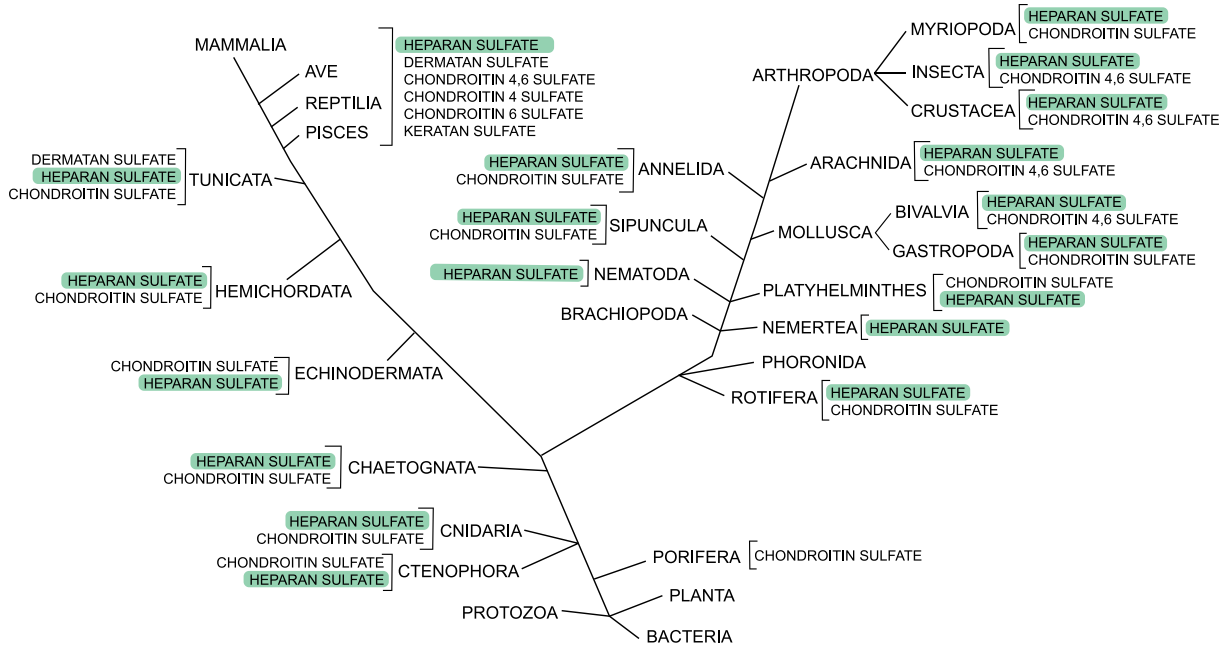

Fig. 1. Heparan sulfates (green) are found in all tissue-organized living organisms across diverse phyla and classes [after Medeiros et al. (10)].

anticoagulant activity arising from binding with antithrombin III (e.g., heparin is commonly used during surgeries or prescribed as a blood thinner) (12). Additionally, heparin influences coagulation pathways by binding to annexin proteins, which are essential for modulating blood clotting, inflammation, and other physiological processes (13, 14). Heparin–annexin interactions occur directly through a Ca^{2+} ion [e.g., annexin II (13)] or via a Ca^{2+}-induced conformational change [e.g., annexin V (15)]. Many GAGs contain similar specific protein-binding sequences, and additional types of GAG–protein interactions continue to be uncovered (9, 16), many of which are Ca^{2+} dependent (3, 17). However, studies of these interactions focus primarily on protein activity, rather than Ca^{2+}–GAG interactions. In all of these processes, the DS and position of the sulfate groups modulate chemical activity.

Ca^{2+}–biomacromolecule interactions are also significant during the biological crystallization of sparingly soluble calcium salts. Minerals such as calcium carbonates and calcium phosphates nucleate and grow within an organic matrix of macromolecules, many of which are sulfated and/ or carboxylated (18–20), and subsequently these minerals aggregate or transform into higher-order structures (e.g., skeletons and shells). Numerous qualitative studies of biomineral systems show that macromolecule composition and structure influence crystal morphology and/or polymorph (8, 18, 20, 21); however, the mechanistic and energetic controls of macromolecules on crystal nucleation are not yet established. A particular shortcoming is the need to understand the interfacial macromolecule–solution environment where crystal nucleation begins and how Ca^{2+}–macromolecule interactions influence crystallization pathways (22–24). These types of interactions may also inform physiological or pathological calcification processes involving calcium phosphates and calcium oxalates (25–27).

For biomedicine and biomineralization systems alike, more studies have investigated Ca^{2+} binding to proteins than to polysaccharides. For many proteins, Ca^{2+} is expected to bind in a conformation-specific manner, whereby the protein must fold to interact with Ca^{2+} (28–33). Upon folding, hydrophobic surfaces become "buried" and release waters of solvation into the bulk; thus, the interactions are entropically driven (5, 32, 34). This entropic release of water is implicated in many systems (35) including protein crystallization (36–38), enzyme regulation (39), micellization (40), biomolecular recognition (41), metal complex formation (including with bio- and synthetic polymers) (42–48), and colloid activity (49).

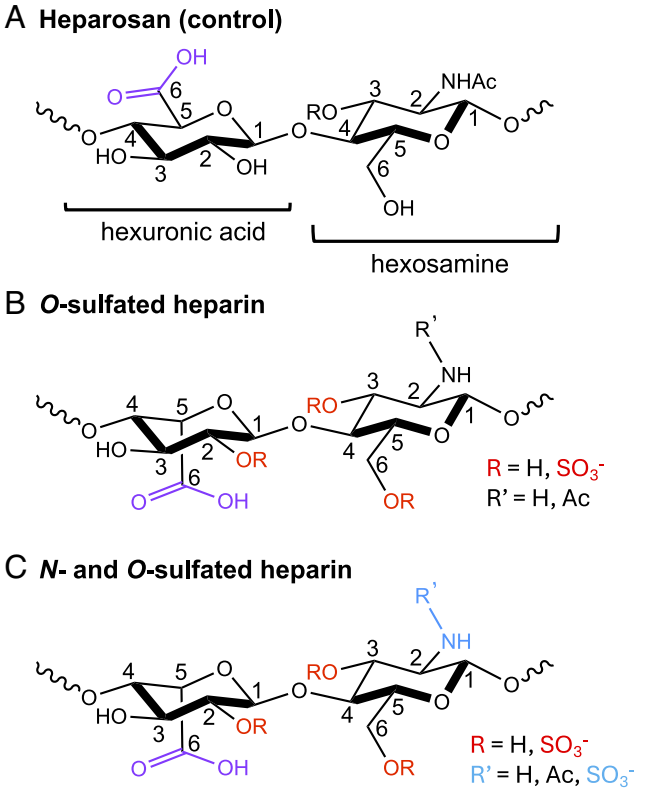

Fig. 2. Chemical structures of polysaccharides used in this study. (*A*) Heparosan, the precursor to heparin, has a disaccharide repeat unit composed of glucuronic acid (GlcA) and glucosamine (GlcN). Heparosan contains only a carboxyl group (at the C6 position of GlcN, purple), allowing it to serve as a nonsulfated control. ~90% of GlcA is epimerized to iduronic acid (IdoA) in heparin. (*B*) The *O*-sulfated heparin only contains SO_3^- at *O*-positions (red): IdoA C2O, GlcN C3O, and GlcN C6O. (*C*) *N*- and *O*-sulfated heparin contains SO_3^- groups at all possible *O*- positions and at the C2N of the GlcN (blue).

Water release and restructuring may also be critical to Ca^{2+}–polysaccharide interactions, though much less is known about this subject. Spectroscopic studies predict Ca^{2+}–GAG binding is coupled with changes to water structure around the polymer, primarily around sulfate groups (50–53). Additional investigations focus on heparin (due to its biomedical significance), leading to some consensus that the C2N-SO_3^- and COO^- substituents of a heparin disaccharide (Fig. 2*C*) are the most significant to cation binding (54–56). However, speculations and disagreements about mechanism(s) persist (57, 58).

Recent studies of Ca^{2+}–heparin interactions primarily utilize spectroscopic (59–64) and computational/theoretical methods that provide additional insight (14, 59–62, 65–67). Through these approaches, researchers conclude the C2N-SO_3^- and COO^- substituents of the disaccharide are significant, and present a Ca^{2+}-specific binding site that is stabilized by C6O-SO_3^- (59–62). They also identify other types of Ca^{2+} interactions that may or may not be site specific, thus indicating Ca^{2+}–heparin interactions could be both localized and delocalized (62, 64–67). However, most studies are hindered by the need for better theoretical models of Ca^{2+} behavior and associated solvation waters, which can dramatically influence interpretations. For example, computational models that treat Ca^{2+} as a sphere of localized charge predict strong selectivity for COO^- groups on heparin (67). In contrast, when the charge on Ca^{2+} is distributed into "dummy centers" to roughly account for ion coordination features, an equal affinity for COO^- and SO_3^- groups is observed (67). Factors such as initial heparin conformation and degree of polymerization also influence the results (60, 65–67). Overall, the structure–property relationships for even this most-studied GAG are not well known, and the roles of associated waters are not well resolved.

Additional evidence for the influence of local water on Ca^{2+}–sulfate and Ca^{2+}–carboxylate interactions is found in kinetic studies of $CaCO_3$ nucleation onto a series of polysaccharides (68, 69). Rate measurements show the energy barrier to $CaCO_3$ crystallization increases with sulfate anion density by a general relationship that includes sulfated and carboxylated macromolecules. The charged groups are postulated to increase polysaccharide hydrophilicity, making crystallization onto the substrate less favorable as water becomes more difficult to displace, thereby increasing the interfacial energy of the polysaccharide–water interface ($\gamma_{PS\text{-}water}$). The findings are consistent with molecular dynamics simulations, showing that Ca^{2+} interactions with polyatomic anions (35, 70–73) and sulfated chitosan derivatives (69) are solvent separated, where the average distance increases with the degree of sulfation for the latter. Hence, the energy barrier to $CaCO_3$ nucleation onto sulfated chitosan derivatives is inversely correlated with S-Ca^{2+} separation (69). Taken together, these studies suggest an underlying systematics whereby the density, type, and position of functional groups influence the solvation of the polysaccharide and Ca^{2+} to modulate ion–macromolecule interactions. In addition to providing a physical basis for how macromolecules regulate the energetics of $CaCO_3$ onto an organic matrix during biomineralization, a general relationship would provide a framework for understanding how Ca^{2+} and similar weakly binding ions interact with macromolecules in diverse contexts, including in biomedical applications.

In this study, we quantify the thermodynamics of Ca^{2+} binding to three heparin-family polysaccharides (Fig. 2 *A*–*C*) using isothermal titration calorimetry (ITC). By determining the thermodynamic profiles of Ca^{2+}–heparin interactions (ΔH_{rxn}, ΔS_{rxn}, ΔG_{rxn}, $K_{binding} = K_b$, reaction stoichiometry) for each material, we show that the binding is composition specific and dependent on sulfate content and position as mediated by water restructuring. These quantitative insights support a recent theoretical model proposing the energy barrier to heterogeneous nucleation of calcite ($CaCO_3$) is heparin-specific due to a systematic and entropically driven consequence of water structuring about Ca^{2+} and their respective functional groups (69). The findings also serve as a model for the thermodynamics of ion binding to other polysaccharides that involve significant water release and restructuring.

1. Results and Discussion

The three heparin-group materials (hereafter referred to as "heparin") were characterized by elemental analysis and ^{1}H NMR (*SI Appendix*, Fig. S1) to quantify the degree of sulfate substitution per disaccharide repeat unit [DS(SO_3^-)] and the relative distribution of sulfate positions. Size exclusion chromatography (*SI Appendix*, Fig. S2) was used to quantify polymer molecular weight. (Table 1). Heparosan (Fig. 2*A*, DS(SO_3^-) = 0) served as a sulfate-free control (74), and two sulfated heparins were used: *O*-sulfated heparin (Fig. 2*B*, DS(SO_3^-) = 1.56) that was chemically modified to remove SO_3^- from the C2N position to present amine groups (C2-NH_2) (75) and *N*- and *O*-sulfated heparin (Fig. 2*C*; DS(SO_3^-) = 2.40) that was unmodified and contained sulfate groups at all naturally possible positions. The *N*- and *O*-sulfated heparin thus presented the highest sulfate density among the investigated materials, and the pK_a was determined via titration (*SI Appendix*, Fig. S3).

ITC was used to measure the thermodynamics of the Ca^{2+}–heparin interactions. Small aliquots of Ca^{2+} were titrated into each polymer solution while measuring the power required to maintain the sample cell at the same temperature as the reference cell (e.g., *SI Appendix*, Fig. S4). The resulting titration curves most closely followed the "independent model" for multiple identical binding

Table 1. Compositions of hexuronic acid and hexosamine monosaccharides of heparin materials in this study

					Hexuronic acid*	Hexosamine*				
Heparin Material	M_w† (kDa)	DP‡	DS(SO_3^-) total*	Total charge*	DS(C2-SO_3^-)	DS(C2N-Ac)	DS(C2N-H_2)	DS(C2N-SO_3^-)	DS(C6O-SO_3^-)	DS(C3O-SO_3^-)
Heparosan	84.0	222	0	−0.99	—	0.94	0.06	—	—	—
O-sulfated heparin	12.4	27	1.56	−2.48	0.62	0.18	0.82	0	0.82	0.12
N- and *O*-sulfated heparin	18.2	36	2.40	−3.38	0.64	0.16	0.12	0.72	0.84	0.24

*Degree of substitution (DS) and total charge values are given per disaccharide repeat unitat pH 8. Sulfate and carboxyl groups have a charge of −1, and each amine has a charge of ~ +0.10, assuming amine pKa ≈ 7 (76).
†M_w = weight average molecular weight.
‡DP = degree of polymerization as the number of disaccharide repeat units; The DP values for the sulfated derivatives assume a sodium counterion.

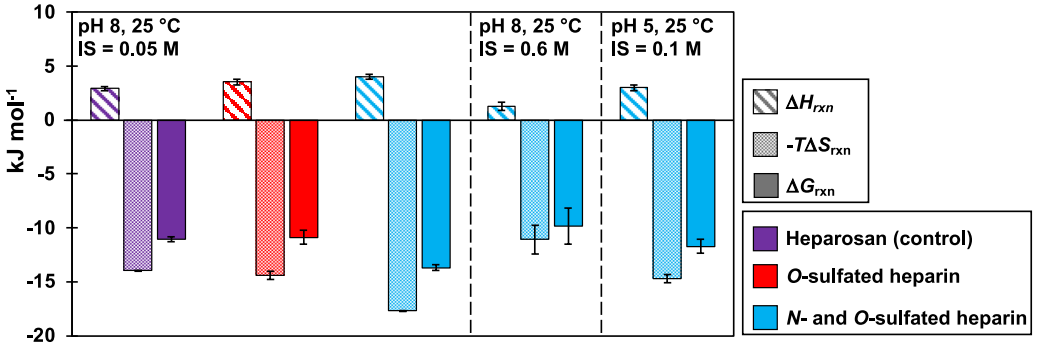

Fig. 3. Thermodynamic parameters for Ca^{2+} binding to each type of heparin material (25 °C). Experiments at pH 8 were performed in a 50 mM tris(hydroxymethyl) aminomethane (tris) buffer. High ionic strength (IS) solutions were adjusted to IS = 0.6 M with NaCl, pH 5 experiments were performed in 100 mM sodium acetate buffer (e.g., *SI Appendix*, Table S1). Error bars represent one SD (σ) of duplicate measurements.

sites (77, 78), enabling us to extract the binding stoichiometry (n, reported as Ca^{2+}:disaccharide), reaction enthalpy (ΔH_{rxn}), and binding constant (K_b) by fitting the peak integration data (heat) versus mole ratio at injection (*SI Appendix*, Fig. S4) for the simplified reaction:

$$n Ca^{2+} + \text{heparin} \overset{K_b}{\rightleftharpoons} Ca\text{-heparin}. \quad [1]$$

The free energy of the reaction (ΔG_{rxn}) and reaction entropy (ΔS_{rxn}) were determined for each type of molecule by the relation:

$$\Delta G_{rxn} = -RT\ln(K_b) = \Delta H_{rxn} - T\Delta S_{rxn}, \quad [2]$$

where R is the universal gas constant, and T is the experimental temperature (298 K). The control experiments (Ca^{2+} into buffer and buffer into heparin material) ensured that any heat exchange not due to a Ca^{2+}–heparin interaction was subtracted before curve fitting. Experimental details, including all ITC thermograms, are provided in *SI Appendix*, *SI Text*, section 1.3, Table S1, and Fig. S5 (60, 72, 73). Additionally, for the *N*- and *O*-sulfated heparin, the effect of ionic strength and pH solution conditions was also investigated. Results are included in figures and discussed in *SI Appendix*, *SI Text*, section 1.3.1.

1.1. Interactions Are Entropically Driven. For all material compositions and solution conditions, the ΔG_{rxn} of the Ca^{2+}–heparin interactions is negative and relatively small in magnitude, consistent with the low free energy associated with many biological systems (5, 6, 79). All interactions are endothermic, indicating coulombic/ electrostatic activity (i.e., charge attraction between Ca^{2+} and COO^-/SO_3^-) alone does not well-describe the binding mechanism (80). The ΔG_{rxn} for each material is dominated by entropic contributions (Fig. 3 and Table 2, and *SI Appendix*, Fig. S2). We therefore conclude that the large ΔS_{rxn} term indicates a mechanism dominated by the favorable release of water molecules whereby the solvation waters (around the polymer and/or Ca^{2+}) are transferred to the bulk solution upon binding. This result is consistent with the idea that Ca^{2+} binding to macromolecules is a consequence of changes in solvation through restructuring (45, 47, 80).

The similarity of the entropically driven Ca^{2+} interactions with heparosan (nonsulfated control) and the *O*-sulfated heparin (Fig. 3, compare purple and red) is surprising given that the SO_3^- groups of the *O*-sulfated heparin increase the charge density of this polysaccharide ~2.5X, relative to heparosan. The thermodynamic parameters are approximately equal within experimental error (e.g. Table 2) which implies carboxyl groups alone are as effective at binding Ca^{2+} as carboxyl and *O*-sulfate groups combined. It is possible the larger molecular weight inherent to heparosan contributes to Ca^{2+} binding (81). However, little difference between the Ca^{2+}-binding activity of an unmodified heparin and an *O*-desulfated heparin (both expected to have low molecular weights) is reported (55). Therefore, we suggest the lack of *N*-sulfates drives the similarity in Ca^{2+} binding for heparosan and *O*-sulfated heparin materials. These results are also consistent with the premise that charge is not the primary driver of Ca^{2+}–heparin interactions.

In contrast to the other materials, the heparin that is both *N*- and *O*-sulfated has the strongest Ca^{2+} interaction (Fig. 3, blue) as predicted by charge per disaccharide. However, small and endothermic contributions of ΔH_{rxn} again indicate that charged groups do not act through coulombic interactions alone during Ca^{2+} interactions but rather as drivers of changes to water structure. The *N*- and *O*-sulfated heparin shows the largest ΔS_{rxn} contribution to ΔG_{rxn}, suggesting that the sulfate group at the *N*-position imposes additional changes to water structuring. However, we do not expect a major difference in solvation structure at the *N*- position compared to *O*-SO_3^- (69), suggesting that the physical origin could arise from a conformational change that impacts hydration, rather than a change in solvation about the NSO_3^- group alone.

Table 2. Thermodynamic parameters determined for each material at 25 °C (Eq. 2) and illustrated in Fig. 3

Material	ΔH_{rxn} ±1 σ (kJ mol^{-1})	$-T\Delta S_{rxn}$ ±1 σ (kJ mol^{-1})	ΔG_{rxn} ±1 σ (kJ mol^{-1})	K_b ±1 σ	n ±1 σ (Ca^{2+} per disaccharide)
Heparosan, pH 8	2.9 ±0.2	−14.0 ±0.1	−11.1 ±0.2	87 ±8	0.35*
O-sulfated heparin, pH 8	3.5 ±0.3	−14.4 ±0.4	−10.9 ±0.6	82 ±21	0.37 ±0.01
N- and *O*-sulfated heparin, pH 8	4.0 ±0.2	−17.7 ±0.1	−13.7 ±0.3	252 ±26	1.05 ±0.07
N- and *O*-sulfated heparin, pH 8, high IS	1.2 ±0.4	−11.1 ±1.3	−9.8 ±1.7	67 ±27	0.9 ±0.2
N- and *O*-sulfated heparin, pH 5	2.0 ±0.3	−14.7 ±0.4	−11.7 ±0.7	116 ±30	1.19 ±0.04

*Manually set to avoid overparameterization during fitting (78).

Clues to the larger ΔS_{rxn} contribution determined for the *N*- and *O*-sulfated heparin may be found in previous studies that monitored shifts in ^{1}H NMR peaks and proposed the NSO_3^- group permits favorable conformation of IdoA residues for Ca^{2+} interactions (55, 82, 83). This suggests *N*- and *O*-sulfated heparin may assume a more favorable conformation for Ca^{2+} interactions than *O*-sulfated heparin. The conformation of the IdoA monosaccharide allowed by the presence of C2N-SO_3^- may create the proposed binding site between NSO_3^- and COO^- groups, dramatically increasing the Ca^{2+} binding ability for *N*- and *O*-sulfated heparin. While these NMR measurements cannot resolve the details of structural changes associated with the released waters (i.e., from where the water is released), they demonstrate the types and positions of functional groups that modify water structure around the polymer during Ca^{2+} interactions.

1.2. Heat Capacity and Entropy of Hydration. As a further test of our interpretation that Ca^{2+}–heparin interactions are driven by the release of water molecules, we determined the change in heat capacity (ΔC_p) for each macromolecule upon Ca^{2+} binding. The heat capacity of solvation water is dependent upon its degree of structuring, and therefore, the ΔC_p upon binding provides a quantitative probe for the degree of water structuring. The utility of ΔC_p for assessing differences in water structure is found in studies of protein folding thermodynamics and the associated hydrophobic effects [e.g., Spolar et al. (32)]. By measuring ΔH_{rxn} using ITC for a series of temperatures (e.g., *SI Appendix*, Table S2), we determine ΔC_p from the relation:

$$\Delta C_p = \frac{\delta \Delta H}{\delta T}. \quad [3]$$

The value of ΔC_p can be interpreted as a measure of the magnitude of water rearrangement upon Ca^{2+} binding or as a change in water-accessible surface area (32, 34). Generally, a positive value represents dehydration of hydrophilic groups ($C_{p,\text{ bulk water}} > C_{p,\text{ solvation waters about metal ions \& polar groups}}$), while a negative value represents dehydration of hydrophobic groups ($C_{p,\text{ bulk water}} < C_{p,\text{ solvation waters about hydrophobic/nonpolar groups}}$) (34, 45, 84–86). Estimates of ΔC_p thus allow us to discern the location from which the majority of solvation waters are released during Ca^{2+} interactions.

For all material compositions, we determined positive values of ΔC_p (Fig. 4*A*), consistent with the idea that these entropically dominated Ca^{2+} interactions primarily involve the release of solvation waters from polar groups and ions (e.g., COO^-, SO_3^-, and/or Ca^{2+}) to the bulk solution, rather than a change in exposed hydrophobic surfaces. Because of the high energy barrier to Ca^{2+} desolvation (87), we assume most of the water restructuring and release occurs about the COO^- and SO_3^- groups, although Ca^{2+} desolvation may also contribute.

Using an approach from the protein binding literature (32, 88–90), measurements of ΔC_p also provide an opportunity to estimate the relative contributions of changes in solvation and conformation to the total entropy change during Ca^{2+}–heparin interactions. The method is generalized for polar/nonpolar solvation and is not specific to amino acids (32, 91), and has been successfully applied to mono- and oligosaccharides (91). Here, we apply it to the heparin-family materials to estimate the relative contributions of these terms. Consider ΔS_{rxn} as a composite of thermal ($\Delta S_{\text{rotational-translational}}$), solvation ($\Delta S_{\text{hydration}}$), and conformation ($\Delta S_{\text{conformation}}$) contributions to the Ca^{2+}–heparin interaction, such that

$$\Delta S_{rxn} = \Delta S_{rotational-translation} + \Delta S_{hydration} + \Delta S_{conformation}. \quad [4]$$

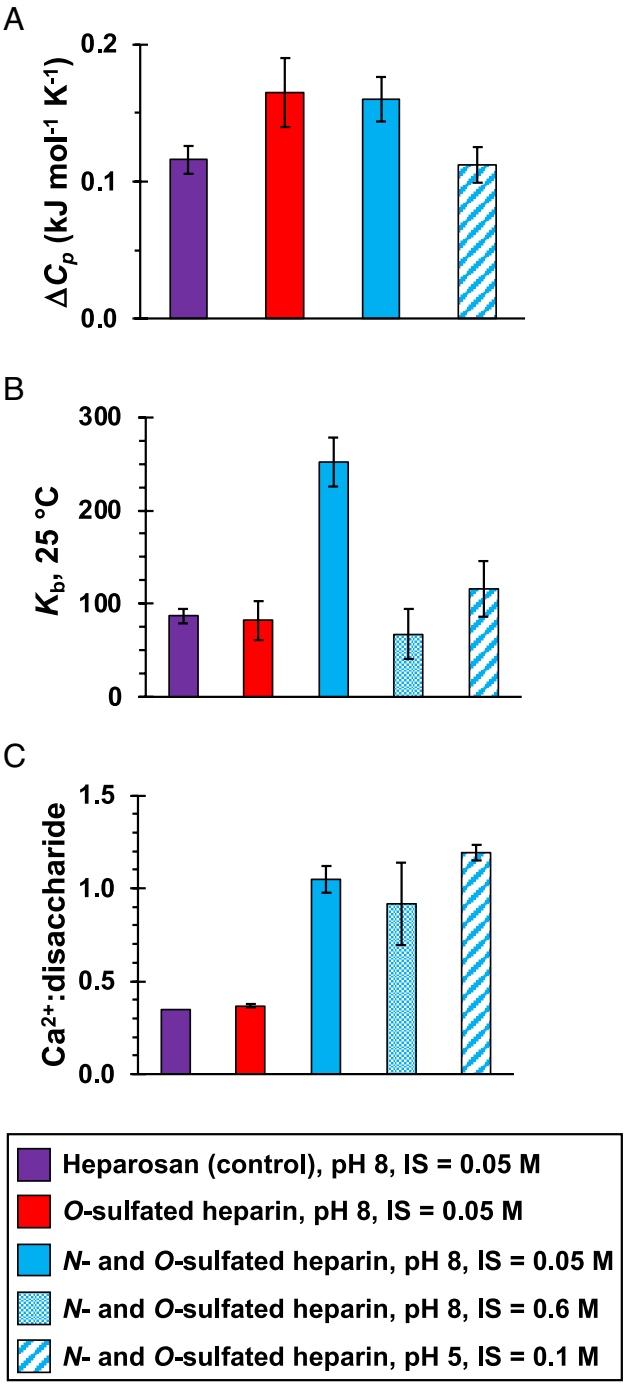

Fig. 4. Comparison of binding parameters for each material. (*A*) Change in heat capacity (ΔC_p) of each material upon heparin interaction with Ca^{2+} (Eqs. **1** and **3**) (*B*) binding constants ($K_{b,}$ 25 °C); (*C*) reaction stoichiometry (Eq. **1**, 25 °C). Error bars represent the SD (σ) of duplicate measurements.

The value of $\Delta S_{\text{rotational-translational}}$ is estimated to be constant in each system (–33.4 J M^{-1} K^{-1}) (91), and

$$\Delta S_{hydration} = \Delta C_p \ln\left(\frac{T}{176\ K}\right), \quad [5]$$

where T is the experimental temperature, and 176 K is the temperature at which polar solvation entropy extrapolates to zero (88–90). Contributions from the $\Delta S_{\text{conformation}}$ term are obtained from (Eq. **4**) by difference.

The summary in *SI Appendix*, Table S3 shows that $\Delta S_{\text{hydration}}$ is the predominant contributor to ΔS_{rxn} (>50%) for all materials at

all solution conditions. This trend supports all studied heparin family molecules interacting with Ca^{2+} by a similar, water-restructuring mechanism. Estimates of $\Delta S_{hydration}$ for the sulfated heparins are >20 J M^{-1} K^{-1} higher than values obtained for the nonsulfated control (heparosan). The difference demonstrates the role of sulfate groups, regardless of position, in modulating desolvation during the interaction.

The estimates also show that contributions from the $\Delta S_{conformation}$ term are material specific. Calcium interactions with heparosan are associated with a favorable $\Delta S_{conformation}$ that comprises ~17% of ΔS_{rxn}. In contrast, low values were found for the sulfated heparins, with $\Delta S_{conformation}$ contributing only ~4 and 7% to Ca^{2+} interactions with *O*-sulfated heparin and *N*- and *O*-sulfated heparin, respectively. Consistent with predictions about iduronic acid conformation (55, 82, 83), the $\Delta S_{conformation}$ is unfavorable for *O*-sulfated heparin and favorable for *N*- and *O*-sulfated heparin, supporting our hypothesis that *N*- and *O*-sulfated heparin adopts a more favorable conformation. The much smaller $\Delta S_{conformation}$ contribution for molecules with sulfate groups concurs with earlier studies that indicate conformation change is not significant to Ca^{2+}–heparin binding (92–94), The higher $\Delta S_{conformation}$ for heparosan may be explained by the low charge density of the molecule allowing the heparosan chain to reconfigure from its starting equilibrium conformation to enable more Ca^{2+}–carboxyl group interactions. The difference between contributions of $\Delta S_{conformation}$ to Ca^{2+} binding with each material also raises mechanistic questions regarding the influence of carboxyl versus sulfate groups on polymer conformation before and after binding interactions.

1.3. Binding Constants and Stoichiometry. Using the thermodynamic profiles determined in this study, we quantify the binding constants (K_b, Fig. 4*B*) and reaction stoichiometry (n = Ca^{2+}:disaccharide, Fig. 4*C*) for each Ca^{2+}–heparin group interaction (e.g., Eq. **1**). All K_b values are relatively small for these low free energy materials and the binding constants for Ca^{2+} interactions with heparosan and *O*-sulfated heparin are similar within experimental errors: K_b = 87 ± 8 and 82 ± 21, respectively. These values are two orders of magnitude smaller than a previous report for Ca^{2+}–alginate interactions (95) and three orders of magnitude smaller than for heavy metal binding to carboxylated polymers (45, 80).

In contrast to the other heparin materials, *N*- and *O*-sulfated heparin exhibits a significantly larger K_b = 252 ± 26, thus demonstrating the importance of the sulfate group at the *N*-position. This K_b is ~3X greater than those of the other materials, but the difference in binding affinities is not proportional to the difference in net charges of the heparosan and *O*-sulfated heparin. The nonlinear relationship between net charge and K_b may be explained by the site-specific interaction enabled by NSO_3^-. The NSO_3^- may enable more favorable orientation and water structuring for Ca^{2+} binding, thus, when the site is lost, so are other interactions that contribute to the larger K_b.

The presence of NSO_3^- groups also influences the binding stoichiometry for Ca^{2+}–heparin interactions. The Ca^{2+}:disaccharide ratio for *N*- and *O*-sulfated heparin is approximately 1:1. This value is consistent with previously reported Ca^{2+}:heparin disaccharide ratio by circular dichroism and NMR methods (54). The value is also consistent with binding at the NSO_3^- site, whereby NSO_3^- and COO^- coordinate Ca^{2+}. The ratio further indicates that even the strongest interactions with heparin do not involve all anionic groups, so do not reach charge parity. This observation is consistent with the seemingly minor contributions of *O*-sulfates to interactions with Ca^{2+}. However, ITC measures only the average stoichiometry of the overall binding interaction. Consequently, the specific binding environment of a given calcium ion (e.g., how many (and what type of) charged groups are associated with Ca^{2+}, or whether the associated charged groups are on the same or different polysaccharide chains) cannot be determined by this technique.

The average binding stoichiometry for the *O*-sulfated heparin is approximately 1:3 Ca^{2+} per disaccharide. A 1:3 ratio indicates that more disaccharide units or anionic groups are necessary to bind Ca^{2+} than would be predicted based on charge parity. Hence, not all anionic groups are involved or able to be involved in the interaction, likely due to restrictions in polymer conformation. One explanation is that *O*-SO_3^- groups can be present in several different positions (C2 of IdoUA, C3 or C6 of GlcN, Fig. 1*B*), as opposed to the *N*-SO_3^- which is always present at the same position (C2 of GlcN). Thus, geometry may contribute more to the stoichiometry. While the value is small, the unfavorable value of $\Delta S_{conformation}$ for *O*-sulfated heparin (e.g., *SI Appendix*, *SI Text*, section 2.2 and Table S3) further supports the reported stoichiometry being a result of conformation effects. To avoid overparameterization during fitting (78), the binding stoichiometry of heparosan was set to 0.35 (*SI Appendix*, *SI Text*, section 1.3). This value was informed in part by the measured binding stoichiometry for *O*-sulfated heparin.

While the evidence shows that the NSO_3^- group has a significant role during binding with Ca^{2+}, these data cannot determine whether the higher K_b and stoichiometry, relative to the other materials, is a direct result of Ca^{2+} interactions with the NSO_3^- group, or a synergistic effect between the *N*- and *O*-sulfates in the same material. To answer this question, one would need to test an only *N*-sulfated heparin while also addressing the synthetic challenge of making this compound (in large enough quantities). Molecular dynamics (MD) simulations of heparins would be a useful alternative to discern these details. For example, a recent MD study of a series of *N*- and/ or *O*-sulfated chitosan materials indicates that the number of water molecules (and HCO_3^- ions) about Ca^{2+} ions is influenced by sulfate position (69).

2. Insights for $CaCO_3$ Nucleation Onto Polysaccharides

Given that the entropic driver of Ca^{2+}–heparin interactions is directly related to changes in solvation at the polysaccharide–solution interface, findings in this study bring insight into the thermodynamic origins of how polysaccharide composition and structure can modulate crystal nucleation onto these substrates. The thermodynamic barrier to forming a critical crystal nucleus of calcite ($CaCO_3$), and other sparingly soluble salts, is controlled by the interfacial free energy of the specific crystallization environment. This term quantifies the free energy required to create a new interface for a given crystal–substrate–solution system (e.g., $CaCO_3$-heparin-H_2O).

To explore this idea, recall that for a polysaccharide (PS)–calcite (cal)–solution (sol) system, the net interfacial energy required to form a new calcite nucleus of critical size, γ_{net}, is a composite term of contributions from three interfaces:

$$\gamma_{net} = \gamma_{cal-sol} + h(\gamma_{cal-PS} - \gamma_{PS-sol}), \quad [6]$$

where h is a nucleus shape factor. Although individual contributions of the three interfaces are not easily resolved, previous studies propose that changes in $\gamma_{PS\text{-}sol}$ are the primary control on γ_{net} (68, 69). They predict that increasingly anionic (hydrophilic) groups reduce $\gamma_{PS\text{-}sol}$, leading to an overall increase in γ_{net} (68, 69). This relationship is supported by a correlation between γ_{net} of calcite nucleation onto diverse polysaccharide compositions and the net charge of those polysaccharides (Fig. 5*A*).

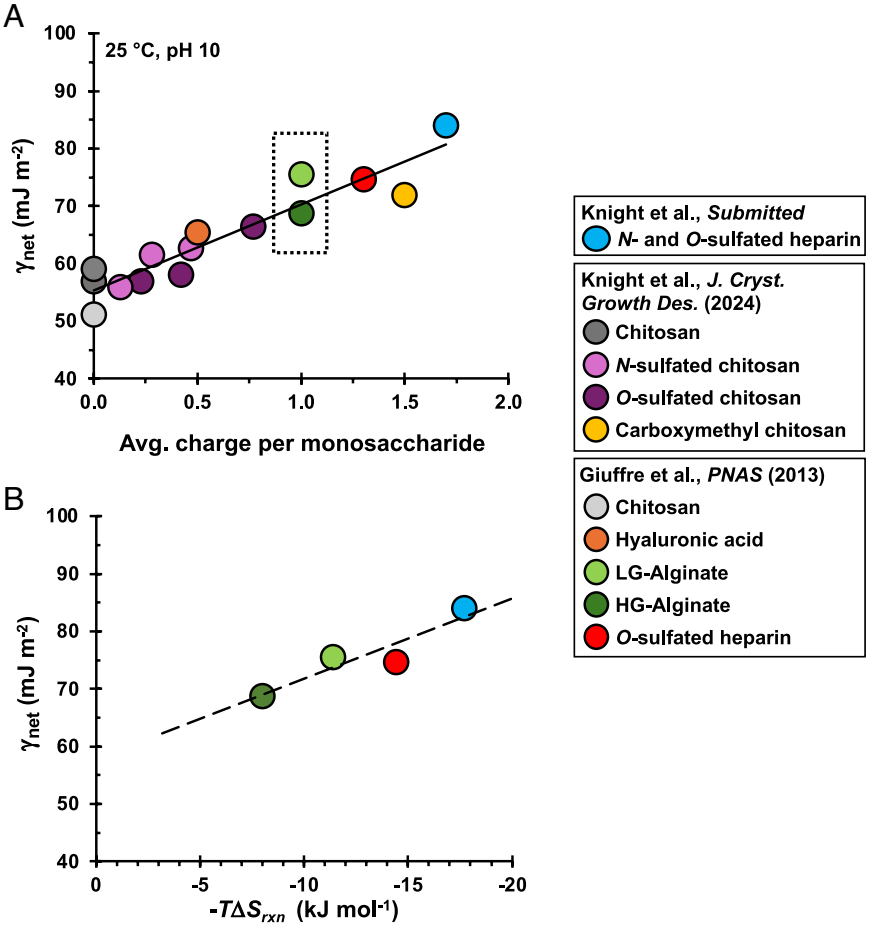

Fig. 5. Measurements suggest an underlying control of water structuring on $CaCO_3$ nucleation and Ca^{2+} binding. (*A*) Energy barrier to calcite nucleation correlates with net charge per monosaccharide across diverse polysaccharides, but charge cannot explain all trends. Note the offset between alginates of the same charge but with different mannuronic: guluronic acid ratios. LG = low guluronic acid block, HG = high guluronic acid block. (*B*) Energy barrier to calcite nucleation correlates with $-T\Delta S_{rxn}$ values determined by ITC of the corresponding molecule with Ca^{2+}. The relationship reconciles the offset between alginates when viewed through the lens of entropic change upon Ca^{2+} interactions. Values shown in this plot are compiled from multiple studies, whereby the $-T\Delta S_{rxn}$ and γ_{net} measurements are for materials that are the same (*N*- and *O*-sulfated heparin), very similar in composition (*O*-sulfated heparin, LG-Alg), or reasonably comparable (HG-Alg) (*SI Appendix*, Tables S5 and S6).

However, Fig. 5*A* also contains data that are offset from the trend, indicating that net charge by itself does not fully explain controls on $CaCO_3$ nucleation. Such deviations suggest other factors, including polysaccharide conformation and/or functional group position, may further "tune" the energy barrier to $CaCO_3$ nucleation. Our findings that Ca^{2+} interactions with heparins are driven by the entropic contribution through water restructuring imply changes in solvation around polar functional groups could underlie the trends and deviations observed in Fig. 5*A*.

For example, the two alginate materials, which have the same net charge but different compositions of mannuronic (M) and guluronic (G) acid residues, have different energy barriers. It is well established that low G-block (LG-Alg) and high G-block (HG-Alg) materials differ in how they coordinate Ca^{2+} (96, 97), and Fang et al. (95) showed (by ITC) that Ca^{2+} interactions with alginates of different M and G compositions present the same ΔG_{rxn} but differ in relative contributions of ΔH_{rxn} and $-T\Delta S_{rxn}$. Thus, the thermodynamic measurements should indicate whether the origin of the offset resides in the differences between their entropic terms during Ca^{2+} interactions. To test this idea, we compared γ_{net} values [this study (*SI Appendix*, Fig. S6) and Giuffre et al. (68)] with corresponding estimates of $-T\Delta S_{rxn}$ [this study and Fang et al. (95)] for two alginate (*SI Appendix*, Table S5) and two heparin materials (*SI Appendix*, Table S6). Indeed, Fig. 5*B* shows a positive correlation such that polysaccharides that present the largest energy barrier to $CaCO_3$ nucleation correspond to the greatest disruption of water structure (most negative $-T\Delta S_{rxn}$) during Ca^{2+} interactions.

Molecular dynamics (MD) simulations of Ca^{2+}–polysaccharide interactions provide additional insights into the relations in Fig. 5*B*. A recent study showed that Ca^{2+} has solvent-separated interactions with SO_3^- and COO^- groups on model chitosan materials. Smaller Ca^{2+}–SO_3^- separations (predicted by MD) correlated with larger thermodynamic barriers to nucleation (experimentally determined) for a series of increasingly sulfated chitosan derivatives (69). The relationship leads us to propose that closer Ca^{2+}–polysaccharide interactions cause greater disruption of solvation water at these sulfated groups which is reflected in a greater entropic contribution to the overall free energy of the binding reaction (Eq. **1**). This explanation is supported by the trend in Fig. 5*B*. One would expect that stronger Ca^{2+} interactions should also correlate with shorter Ca^{2+}–functional group distances (and therefore higher energy barriers); however, a correlation between γ_{net} and K_b is not observed for the alginates. This raises the question of relative contributions of hydrophilic interactions and Ca^{2+} binding mechanism to functional groups to control the parameters in γ_{net}. It also raises the possibility that $-T\Delta S_{rxn}$ is predictive only within groups of likematerials. For example, it is plausible that Fig. 5*B* contains two material-specific trends: one for heparins and one for alginates. Overall, the trends in Fig. 5 *A* and *B* suggest that an underlying systematics whereby the thermodynamics of Ca^{2+}–polymer interactions, as well as energetic barriers to $CaCO_3$ nucleation, are rooted in the details of solvation at interfaces for both processes.

3. Evidence for Systematics in Ca^{2+}–Biomolecule Interactions

Findings from this study of three heparin-family molecules present an opportunity to probe broader questions regarding the nature of Ca^{2+}–polysaccharide interactions and implications

for biological systems. First, Ca^{2+} interactions with heparins and some other anionic polysaccharides share an underlying thermodynamic signature that is independent of macromolecule charge. By compiling measurements of Ca^{2+} interactions with (the few) published values for linear, anionic polysaccharides (*SI Appendix*, Table S7) (95, 98–100), Fig. 6*A* shows a shared ratio of $-T\Delta S_{rxn}/\Delta G_{rxn}$ in the range of 1.25 to 1.50 that is constant across average charge of the monosaccharide. The near/ greater than unity value of $-T\Delta S_{rxn}/\Delta G_{rxn}$ is an expected consequence for systems that have a larger entropic contribution to Ca^{2+} interactions relative to enthalpic contribution. However, not all ΔH_{rxn} values are small and near-constant (*SI Appendix*, Table S7). The similar ratio for multiple types of polysaccharides and conditions suggests a general theme for Ca^{2+}–polysaccharide interactions and may provide a tool for estimating thermodynamic properties of similar systems for which no data are available.

Second, deviations from the trend in Fig. 6*A* appear to illustrate additional types of Ca^{2+}–polysaccharide interactions and reiterate gaps in our thermodynamic understanding of ion binding to polysaccharides. Published measurements for some Ca^{2+}–polygalacturonate (99) interactions as well as some Ca^{2+}–alginate (95) studies show lower $-T\Delta S_{rxn}/\Delta G_{rxn}$ ratios of ~0.50 (Fig. 6*A*). The offsets may arise from how these materials can crosslink via Ca^{2+} and thus are associated with a greater enthalpic contribution. In the case of polygalacturonate (99), Ca^{2+} binding begins with an entropic interaction ("step 1") consistent with what is seen for other polysaccharides. This is followed by crosslinking between chains ("step 2"), which likely correlates with a conformational change that may not involve significant water rearrangement or release. For the alginates, an entropic step 1 binding stage was also observed, but it was too rapid to be quantified (95). Thus, the lower $-T\Delta S_{rxn}/\Delta G_{rxn}$ values for alginates represent the step 2 crosslinking energetics.

Third, the thermodynamic profiles reported in this study reiterate the low free energy of ion binding reactions that are associated with most biological activity (5, 6, 79). Jimenez and Benitez (6) postulate that a biologically functional range of ΔG_{rxn} for protein–ligand interactions is maintained by evolutionary adaptations that have resulted in an enthalpy–entropy compensation relationship. Although polysaccharides and proteins differ significantly in their structures and functions, they share critical "universalities" such as polymerization mechanism and higher-order assembly (101).

The relationships for proteins lead us to ask if Ca^{2+} interactions with polysaccharides also exhibit enthalpy–entropy compensation. Values of $-T\Delta S_{rxn}$ for Ca^{2+}–polysaccharide interactions are linearly correlated with ΔH_{rxn} to give a slope ~2 (Fig. 6*B*). The trend includes all polysaccharides in Fig. 6*A* except the outliers discussed above, likely for similar reasons. The ΔG_{rxn} values range from approximately 10 to 30 kJ mol^{-1}. To put the relationship for polysaccharides into perspective, Fig. 6*B* shows that Ca^{2+} interactions with proteins also exhibit an entropy–enthalpy compensation trend, but with a slope of ~1. The lower slope, compared to polysaccharides, indicates a stronger energetic compensation whereby the relative changes in entropy and enthalpy are more balanced and correspond to a smaller ΔG_{rxn} range of 25 to 30 kJ mol^{-1}. This result is consistent with how water restructuring during Ca^{2+}–protein interactions couples with greater conformation changes to result in a larger change to the ΔH_{rxn} contribution, relative to polysaccharides. We acknowledge the protein data shown here (*SI Appendix*, Table S7) do not represent an exhaustive search of protein thermodynamic measurements; however, they do represent diverse compositions that include cow milk proteins (30), soy proteins (29), a mutant human lysozyme (28), calmodulin (31), and homogeneous polypeptides (81), A few proteins are offset from the trend, suggesting these Ca^{2+} interactions may or may not involve conformation change. The crosslinking polysaccharides

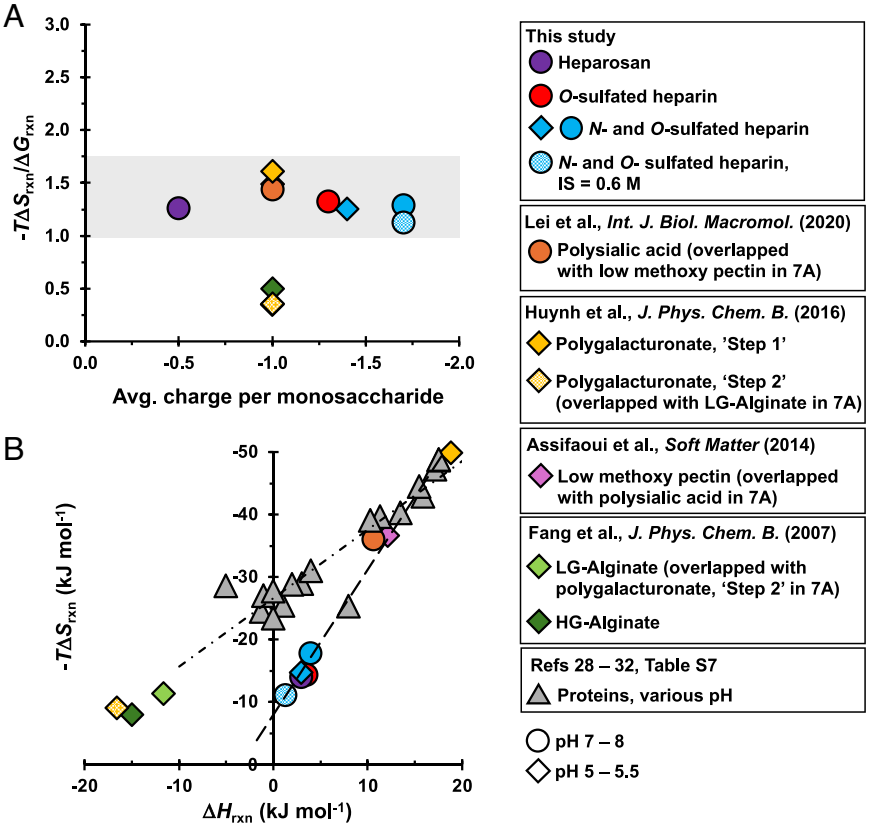

Fig. 6. Compilation of thermodynamic measurements for Ca^{2+} binding to heparins and other polysaccharides shows: (*A*) Ratio of entropic contributions to the free energy of Ca^{2+} binding, $-T\Delta S_{rxn}/\Delta G_{rxn}$, is independent of the average charge per monosaccharide for diverse polysaccharides (gray band). Most values are 1.25 to 1.50; however, a larger band is shaded (1.00 to 1.75) to highlight all relevant data points in this group. The near/ greater than unity ratio reflects their entropically dominated interactions with Ca^{2+}. Offsets from this trend indicate other types of Ca^{2+}–polysaccharide binding (see text). (*B*) Ca^{2+} interactions with polysaccharides exhibit an entropy–enthalpy compensation relationship with a slope of ~2. The trend found for polysaccharides is distinct from that of proteins (slope of ~1). Note: LG = low guluronic acid, HG = high guluronic acid, IS = ionic strength.

that appeared as offsets in Fig. 6*A* would seem to correlate with the protein trend. Taken together, it is plausible the distinct trends in Fig. 6*B* represent when Ca^{2+} interactions are dominated only by water restructuring (slope ~2) or coupled to a conformational change (slope ~1), independent of biopolymer class.

4. Conclusions

This quantitative study demonstrates the thermodynamics of calcium binding is the consequence of entropically driven water restructuring that occurs during Ca^{2+} interactions with different types and positions of functional groups. Through a systematic approach, we show that Ca^{2+} binding to the *N*- and *O*- sulfated heparin biomolecule is significantly stronger than to *O*-sulfated heparin and the nonsulfated heparosan control. This finding demonstrates the importantance of the NSO_3^- group/position in modulating Ca^{2+} interactions and provides a physical basis for understanding its activity during biological processes and for optimizing activity in biomedical systems.

The significance of water restructuring during calcium ion interactions with macromolecules emerges as a general theme for understanding diverse, biologically relevant systems. For biomineralization, the data show that a large $-T\Delta S_{rxn}$ upon Ca^{2+} binding correlates with high interfacial energy (γ_{net}) to calcite nucleation, independently supporting the model that polysaccharide-specific controls on the kinetics of $CaCO_3$ nucleation (and possibly other Ca-bearing biominerals) are driven by changes in water structuring.

When the thermodynamic profiles determined for Ca^{2+} interactions with heparins are combined with data reported for other charged polysaccharides, we find an enthalpy–entropy compensation relationship that reflects how the large $-T\Delta S_{rxn}$ contribution to the total free energy of the reaction is not coupled to a conformational change. In contrast, data from published measurements of Ca^{2+}–protein binding thermodynamics present a different compensation signature that indicates a combination of changes in molecular conformation and solvation. The relationships suggest a tool for predicting the thermodynamics of Ca^{2+} binding to macromolecules in biochemical and materials systems for which there are no experimental data. The relations also provide insights into the evolutionary adaptations that shaped low free energy Ca^{2+}–biopolymer activity and structure–function relations across early living systems.

5. Materials and Methods

Heparosan was produced and purified as described by Wang et al. (74). The *O*-sulfated heparin was chemically modified to remove SO_3^- from the C_2N position using established methods (75). The *N*- and *O*-sulfated heparin was obtained as a purified, natural porcine sample. Detailed descriptions of materials and their characterization are provided in *SI Appendix*, *SI Text*, sections 1.1 and 1.2. The ITC instrument used was an Affinity-ITC (TA Instruments), and details for each experiment are provided in *SI Appendix*, *SI Text*, section 1.3. $CaCO_3$ nucleation rates onto *N*- and *O*-sulfated heparin were measured using established methods (68, 69) and are described in *SI Appendix*, *SI Text*, section 1.4.

Data, Materials, and Software Availability. All study data are included in the article and/or *SI Appendix*.

ACKNOWLEDGMENTS. This project was funded by the United States Department of Energy Office of Basic Energy Sciences (OBES), Division of Chemical Sciences, Geosciences and Biosciences through award DE FG02-00ER15112 (to P.M.D.), and by OBES under Award Number DE-SC0023035 (to M.D.S). This work was also supported (to K.J.E.) by GlycoMIP, a NSF Materials Innovation Platform funded through Cooperative Agreement DMR-1933525. We thank Jim De Yoreo, Alexandra Navrotsky, and Ming Zhang for helpful comments on the manuscript, Fuming Zhang and Jonathan Dordick at Rensselaer Polytechnic Institute for supplying heparosan materials, and the late Robert J. Linhardt for his unparalleled contributions to heparin research.

Author affiliations: [a]Department of Chemistry, Virginia Tech, Blacksburg, VA 24061; [b]Macromolecules Innovation Institute, Virginia Tech, Blacksburg, VA 24061; [c]Department of Sustainable Biomaterials, Virginia Tech, Blacksburg, VA 24061; [d]GlycoMIP, Virginia Tech, Blacksburg, VA 24061; [e]Department of Geosciences, Virginia Tech, Blacksburg, VA 24061; and [f]Department of Materials Sciences and Engineering, Virginia Tech, Blacksburg, VA 24061

Author contributions: B.M.K., C.M.B.G., M.D.S., K.J.E., and P.M.D. designed research; B.M.K., C.M.B.G., and C.D.M. performed research; B.M.K., C.M.B.G., M.D.S., K.J.E., C.D.M., and P.M.D. analyzed data; and B.M.K., C.M.B.G., M.D.S., K.J.E., C.D.M., C.A.M., and P.M.D. wrote the paper.

1. R. J. P. Williams, Biochemistry of sodium, potassium, magnesium, and calcium. *Q. Rev.* **24**, 331 (1970).
2. J. G. McCormack, A. P. Halestrap, R. M. Denton, Role of calcium-ions in regulation of mammalian intramitochondrial metabolism. *Physiol. Rev.* **70**, 391–425 (1990).
3. I. Capila, R. J. Linhardt, Heparin - protein interactions. *Angew. Chem.* **41**, 391–412 (2002).
4. R. M. Denton, Regulation of mitochondrial dehydrogenases by calcium ions. *Biochim. et Biophy. Acta-Bioener.* **1787**, 1309–1316 (2009).
5. K. Sharp, Entropy-enthalpy compensation: Fact or artifact?. *Protein Sci.* **10**, 661–667 (2001).
6. J. S. Jiménez, M. J. Benítez, Gibbs free energy and enthalpy-entropy compensation in protein-ligand interactions. *Biophysica* **4**, 298–309 (2024).
7. E. Ruoslahti, Y. Yamaguchi, Proteoglycans as modulators of growth factor activities. *Cell* **64**, 867–869 (1991).
8. A. Rao, J. K. Berg, M. Kellermeier, D. Gebauer, Sweet on biomineralization: Effects of carbohydrates on the early stages of calcium carbonate crystallization. *Eur. J. Mineral.* **26**, 537–552 (2014).
9. S. Ricard-Blum *et al.*, A biological guide to glycosaminoglycans: Current perspectives and pending questions. *FEBS J.* **291**, 3331–3366 (2024).
10. G. F. Medeiros *et al.*, Distribution of sulfated glycosaminoglycans in the animal kingdom: Widespread occurrence of heparin-like compounds in invertebrates. *Biochim. et Biophys. Acta-General Sub.* **1475**, 287–294 (2000).
11. H. B. Nader *et al.*, Heparan sulfates and heparins: Similar compounds performing the same functions in vertebrates and invertebrates?. *Braz. J. Med. Biol. Res.* **32**, 529–538 (1999).
12. J. Hirsh, S. S. Anand, J. L. Halperin, V. Fuster, Guide to anticoagulant therapy: Heparin. *Arterioscler. Thromb. Vasc. Biol.* **21**, e9–e9 (2001).
13. C. Shao *et al.*, Crystallographic analysis of calcium-dependent heparin binding to annexin A2*. *J. Biol. Chem.* **281**, 31689–31695 (2006).
14. M. M. Kogut, M. Maszota-Zieleniak, M. Marcisz, S. A. Samsonov, Computational insights into the role of calcium ions in protein–glycosaminoglycan systems. *Phys. Chem. Chem. Phys.* **23**, 3519–3530 (2021).
15. I. Capila, V. A. VanderNoot, T. R. Mealy, B. A. Seaton, R. J. Linhardt, Interaction of heparin with annexin V. *FEBS Lett.* **446**, 327–330 (1999).
16. E. S. Place, N. D. Evans, M. M. Stevens, Complexity in biomaterials for tissue engineering. *Nat. Mater.* **8**, 457–470 (2009).
17. P. Sionkowski *et al.*, Effect of ion and binding site on the conformation of chosen glycosaminoglycans at the albumin surface. *Entropy* **24**, 811 (2022).
18. H. A. Lowenstam, S. Weiner, *On Biomineralization* (Oxford University Press, 1989).
19. E. R. Wise *et al.*, The organic−mineral interface in bone is predominantly polysaccharide. *Chem. Mater.* **19**, 5055–5057 (2007).
20. B. M. Knight, K. J. Edgar, J. J. De Yoreo, P. M. Dove, Chitosan as a canvas for studies of macromolecular controls on CaCO3 biological crystallization. *Biomacromolecules* **24**, 1078–1102 (2023).
21. C. A. McCutchin, K. J. Edgar, C.-L. Chen, P. M. Dove, Silica-biomacromolecule interactions: Toward a mechanistic understanding of silicification. *Biomacromolecules* **26**, 43–84 (2025).
22. P. J. M. Smeets, K. R. Cho, R. G. E. Kempen, N. A. J. M. Sommerdijk, J. J. De Yoreo, Calcium carbonate nucleation driven by ion binding in a biomimetic matrix revealed by in situ electron microscopy. *Nat. Mater.* **14**, 394–399 (2015).
23. S. E. Gleeson, S. Kim, T. Yu, M. Marcolongo, C. Y. Li, Insight on the role of poly(acrylic acid) for directing calcium phosphate mineralization of synthetic polymer bone scaffolds. *ACS Appl. Bio Mater.* **5**, 4493–4503 (2022).
24. F. A. Davila-Hernandez *et al.*, Directing polymorph specific calcium carbonate formation with de novo protein templates. *Nat. Commun.* **14**, 8191 (2023).
25. S. Boonrungsiman *et al.*, The role of intracellular calcium phosphate in osteoblast-mediated bone apatite formation. *Proc. Natl. Acad. Sci.* **109**, 14170-14175 (2012).
26. D. S. Goldfarb *et al.*, Effect of hydroxycitrate (HCA) on urine chemistry in calcium kidney stone formers. *J. Am. Soc. Nephrol.* **32**, 225–225 (2021).
27. D. Kim *et al.*, Bio-inspired multifunctional disruptors of calcium oxalate crystallization. *Nat. Commun.* **16**, 5229 (2025).
28. R. Kuroki, S. Kawakita, H. Nakamura, K. Yutani, Entropic stabilization of a mutant human lysozyme induced by calcium-binding. *Proc. Natl. Acad. Sci. U.S.A.* **89**, 6803–6807 (1992).
29. L.-S. Canabady-Rochelle, C. Sanchez, M. Mellema, S. Banon, Study of calcium−soy protein interactions by isothermal titration calorimetry and pH cycle. *J. Agric. Food Chem.* **57**, 5939–5947 (2009).
30. L. S. Canabady-Rochelle, C. Sanchez, M. Mellema, S. Banon, Thermodynamic characterization of calcium-milk protein interaction by isothermal titration calorimetry. *Dairy Sci. Technol.* **89**, 257–267 (2009).

31. M. R. Beccia *et al.*, Thermodynamics of calcium binding to the calmodulin N-terminal domain to evaluate site-specific affinity constants and cooperativity. *J. Biol. Inorg. Chem.* **20**, 905–919 (2015).
32. R. S. Spolar, M. T. Record, Coupling of local folding to site-specific binding of proteins to DNA. *Science* **263**, 777–784 (1994).
33. J. S. Ren, T. C. Jenkins, J. B. Chaires, Energetics bf DNA intercalation reactions. *Biochemistry* **39**, 8439–8447 (2000).
34. B. Madan, K. Sharp, Molecular origin of hydration heat capacity changes of hydrophobic solutes: Perturbation of water structure around alkanes. *J. Phys. Chem. B* **101**, 11237–11242 (1997).
35. M. Kellermeier *et al.*, Entropy drives calcium carbonate ion association. *ChemPhysChem* **17**, 3535–3541 (2016).
36. P. L. Privalov, G. I. Makhatadze, Contribution of hydration to protein–folding thermodynamics. 2. The entropy and gibbs energy of hydration. *J. Mol. Biol.* **232**, 660–679 (1993).
37. P. G. Vekilov *et al.*, Intermolecular interactions, nucleation, and thermodynamics of crystallization of hemoglobin C. *Biophys. J.* **83**, 1147–1156 (2002).
38. M. Kinoshita, Importance of translational entropy of water in biological self-assembly processes like protein folding. *Int. J. Mol. Sci.* **10**, 1064–1080 (2009).
39. M. F. Colombo, D. C. Rau, V. A. Parsegian, Protein solvation in allosteric regulation – A water effect on hemoglobin. *Science* **256**, 655–659 (1992).
40. S. Paula, W. Sus, J. Tuchtenhagen, A. Blume, Thermodynamics of micelle formation as a function of temperature – a high-sensitivity titration calorimetry study. *J. Phys. Chem.* **99**, 11742–11751 (1995).
41. P. W. Snyder *et al.*, Mechanism of the hydrophobic effect in the biomolecular recognition of arylsulfonamides by carbonic anhydrase. *Proc. Natl. Acad. Sci. U.S.A.* **108**, 17889–17894 (2011).
42. P. Prapaipong, E. L. Shock, C. M. Koretsky, Metal–organic complexes in geochemical processes: Temperature dependence of the standard thermodynamic properties of aqueous complexes between metal cations and dicarboxylate ligands. *Geochim. Cosmochim. Acta* **63**, 2547–2577 (1999).
43. W. R. Archer *et al.*, Synthesis and rare-earth-element chelation properties of linear poly(ethylenimine methylenephosphonate). *Macromolecules* **53**, 2061–2068 (2020).
44. A. M. Ponsiglione, M. Russo, E. Torino, Glycosaminoglycans and contrast agents: The role of hyaluronic acid as MRI contrast enhancer. *Biomolecules* **10**, 1612 (2020).
45. W. R. Archer, C. M. B. Gallagher, V. Vaissier Welborn, M. D. Schulz, Exploring the role of polymer hydrophobicity in polymer–metal binding thermodynamics. *Phys. Chem. Chem. Phys.* **24**, 3579–3585 (2022).
46. P. Werner *et al.*, Investigating the role of sulfate groups for the binding of Gd3+ ions to glycosaminoglycans with NMR relaxometry. *ChemMedChem* **17**, e202100764 (2022).
47. V. V. Welborn, W. R. Archer, M. D. Schulz, Characterizing ion-polymer interactions in aqueous environment with electric fields. *J. Chem. Inf. Model.* **63**, 2030–2036 (2023).
48. A. Glisman *et al.*, Multivalent ion-mediated polyelectrolyte association and structure. *Macromolecules* **57**, 1941–1949 (2024).
49. P. F. Damasceno, M. Engel, S. C. Glotzer, Crystalline assemblies and densest packings of a family of truncated tetrahedra and the role of directional entropic forces. *ACS Nano* **6**, 609–614 (2012).
50. D. Grant, C. F. Moffat, W. F. Long, F. B. Williamson, Altered water-structure in mixtures of heparin and metal–ions. *Biochem. Soc. Trans.* **12**, 302–302 (1984).
51. D. Grant, W. F. Long, F. B. Williamson, Infrared-spectroscopy of heparin cation complexes. *Biochem. J.* **244**, 143–149 (1987).
52. D. Grant, W. F. Long, F. B. Williamson, The dependence on counter-cation of the degree of hydration of heparin. *Biochem. Soc. Trans.* **18**, 1283–1284 (1990).
53. D. Grant, W. F. Long, C. F. Moffat, F. B. Williamson, A study of ca2+-heparin complex-formation by polarimetry. *Biochem. J.* **282**, 601–604 (1992).
54. J. N. Liang, B. Chakrabarti, L. Ayotte, A. S. Perlin, An essential role for the 2-sulfamino group in the interaction of calcium-ion with heparin. *Carbohydr. Res.* **106**, 101–109 (1982).
55. L. Ayotte, A. S. Perlin, NMR spectroscopic observations related to the function of sulfate groups in heparin – calcium-binding vs biological-activity. *Carbohydr. Res.* **145**, 267–277 (1986).
56. D. Grant, W. F. Long, F. B. Williamson, N. E. Woodhead, A study by equilibrium dialysis suggests the occurrence of 2 types of heparin-Ca^{2+} interaction. *Ircs Med. Sci. Biochem.* **14**, 805–806 (1986).
57. M. B. Mathews, Structural factors in cation binding to anionic polysaccharides of connective tissue. *Arch. Biochem. Biophys.* **104**, 394 (1964).
58. M. A. Swairjo, N. O. Concha, M. A. Kaetzel, J. R. Dedman, B. A. Seaton, Ca2+-bridging mechanism and phospholipid head group recognition in the membrane-binding protein annexin-V. *Nat. Struct. Biol.* **2**, 968–974 (1995).
59. F. Chevalier, J. Angulo, R. Lucas, P. M. Nieto, M. Martín-Lomas, The heparin-Ca2+ interaction: Structure of the Ca2+ binding site. *Eur. J. Org. Chem.* **2002**, 2367–2376 (2002).
60. F. Chevalier, R. Lucas, J. Angulo, M. Martin-Lomas, P. M. Nieto, The heparin–Ca2+ interaction: The influence of the O-sulfation pattern on binding. *Carbohydr. Res.* **339**, 975–983 (2004).
61. M. Hricovíni, Effect of solvent and counterions upon structure and NMR spin—spin coupling constants in heparin disaccharide. *J. Phys. Chem. B* **115**, 1503–1511 (2011).
62. D. Ortiz, Q. Enjalbert, L. MacAleese, P. Dugourd, J.-Y., Salpin, Effects of calcium complexation on heparin-like disaccharides. A combined theoretical, tandem mass spectrometry and ultraviolet experiment. *Rapid Commun. Mass Spectrom.* **29**, 1135–1144 (2015).
63. C. J. Gray *et al.*, Applications of ion mobility mass spectrometry for high throughput, high resolution glycan analysis. *Biochim. et Biophysic. Acta (BBA) - General Subj.* **1860**, 1688-1709 (2016).
64. D. Sieme, C. Griesinger, N. Rezaei-Ghaleh, Metal binding to Sodium Heparin monitored by quadrupolar NMR. *Int. J. Mol. Sci.* **23**, 13185 (2022).
65. M. Remko, P. T. Van Duijnen, R. Broer, Effect of metal ions (Li+, Na+, K+, Mg2+ and Ca2+) and water on the conformational changes of glycosidic bonds in heparin oligosaccharides. *RSC Adv.* **3**, 9843–9853 (2013).
66. M. Remko, R. Broer, A. Remková, P. T. Van Duijnen, How strong are Ca2+–heparin and Zn2+–heparin interactions?. *Chem. Phys. Lett.* **621**, 12–17 (2015).
67. M. M. Kogut, A. Danielsson, S. Ricard-Blum, S. A. Samsonov, Impact of calcium ions on the structural and dynamic properties of heparin oligosaccharides by computational analysis. *Comput. Biol. Chem.* **99**, 107727 (2022).
68. A. J. Giuffre, L. M. Hamm, N. Han, J. J. De Yoreo, P. M. Dove, Polysaccharide chemistry regulates kinetics of calcite nucleation through competition of interfacial energies. *Proc. Natl. Acad. Sci. U.S.A.* **110**, 9261–9266 (2013).
69. B. M. Knight *et al.*, Kinetics of calcite nucleation onto sulfated chitosan derivatives and implications for water-polysaccharide interactions during crystallization of sparingly soluble salts. *Crystal Growth Design* **24**, 6338–6353 (2024).
70. H. J. Li *et al.*, Insights into water-mediated ion clustering in aqueous CaSO4 solutions: Pre-nucleation cluster characteristics studied by *ab initio* calculations and molecular dynamics simulations. *Phys. Chem. Chem. Phys.* **19**, 11390–11403 (2017).
71. E. H. Byrne, P. Raiteri, J. D. Gale, Computational insight into calcium–sulfate ion pair formation. *J. Physic. Chem. C* **121**, 25956–25966 (2017).
72. X. W. Wang *et al.*, Density functional theory based molecular dynamics study of solution composition effects on the solvation shell of metal ions. *Phys. Chem. Chem. Phys.* **22**, 16301–16313 (2020).
73. J.-N. Boyn, E. A. Carter, Characterizing the mechanisms of Ca and Mg carbonate ion-pair formation with multi-level molecular dynamics/quantum mechanics simulations. *J. Phys. Chem. B* **127**, 10824–10832 (2023).
74. Z. Wang *et al.*, E. coli K5 fermentation and the preparation of heparosan, a bioengineered heparin precursor. *Biotechnol. Bioeng.* **107**, 964–973 (2010).
75. Y. Inoue, K. Nagasawa, Selective N-desulfation of heparin with dimethyl sulfoxide containing water or methanol. *Carbohydr. Res.* **46**, 87–95 (1976).
76. C. N. Beecher, C. K. Larive, 1H and 15N NMR characterization of the amine groups of heparan sulfate related glucosamine monosaccharides in aqueous solution. *Anal. Chem.* **87**, 6842–6848 (2015).
77. T. Wiseman, S. Williston, J. F. Brandts, L.-N. Lin, Rapid measurement of binding constants and heats of binding using a new titration calorimeter. *Anal. Biochem.* **179**, 131–137 (1989).
78. W. B. Turnbull, A. H. Daranas, On the value of *c*: Can low affinity systems be studied by isothermal titration calorimetry?. *J. Am. Chem. Soc.* **125**, 14859–14866 (2003).
79. M. E. Dixon, T. K. Hitchens, R. G. Bryant, Comparisons of pressure and temperature activation parameters for amide hydrogen exchange in T4 lysozyme. *Biochemistry* **39**, 248–254 (2000).
80. C. G. Sinn, R. Dimova, M. Antonietti, Isothermal titration calorimetry of the polyelectrolyte/water interaction and binding of Ca2+: Effects determining the quality of polymeric scale inhibitors. *Macromolecules* **37**, 3444–3450 (2004).
81. M. B. Gindele, K. K. Malaszuk, C. Peter, D. Gebauer, On the binding mechanisms of calcium ions to polycarboxylates: Effects of molecular weight, side chain, and backbone chemistry. *Langmuir* **38**, 14409–14421 (2022).
82. D. Grant, W. F. Long, C. F. Moffat, F. B. Williamson, Infrared-spectroscopy of heparins suggests that the region 750–950 cm-1 is sensitive to changes in iduronate residue ring conformation. *Biochem. J.* **275**, 193–197 (1991).
83. B. Mulloy *et al.*, The effect of variation of substitution on the solution conformation of heparin: A spectroscopic and molecular modelling study. *Carbohydr. Res.* **255**, 1–26 (1994).
84. G. E. Boyd, Q. V. Larson, S. Lindenba, Heat capacity changes in ion-exchange reactions. Exchange of tera-n-butylammonium with sodium ion in cross-linked polystyrenesulfonate. *J. Phys. Chem.* **72**, 2651 (1968).
85. D. Chandler, Interfaces and the driving force of hydrophobic assembly. *Nature* **437**, 640–647 (2005).
86. J. C. Foster *et al.*, 100th anniversary of macromolecular science viewpoint: The role of hydrophobicity in polymer phenomena. *ACS Macro Lett.* **9**, 1700–1707 (2020).
87. D. Langmuir, *Aqueous Environmental Geochemistry* (Prentice Hall, Upper Saddle River, N.J., 1997), pp. 82–118.
88. R. L. Baldwin, Temperature dependence of the hydrophobic interaction in protein folding. *Proc. Natl. Acad. Sci. U.S.A.* **83**, 8069-8072 (1986).
89. G. I. Makhatadze, P. L. Privalov, Contribution of hydration to protein folding thermodynamics: I. The enthalpy of hydration. *J. Mol. Biol.* **232**, 639–659 (1993).
90. J. A. Caro *et al.*, Entropy in molecular recognition by proteins. *Proc. Natl. Acad. Sci. U.S.A.* **114**, 6563–6568 (2017).
91. M. Nagao, Y. Hoshino, Y. Miura, Quantification of thermodynamic effects of carbohydrate multivalency on avidity using synthetic discrete glycooligomers. *Chem. Commun.* **60**, 7021–7024 (2024).
92. B. Lages, S. S. Stivala, Interaction of polyelectrolyte heparin with copper(II) and calcium. *Biopolymers* **12**, 127–143 (1973).
93. M. C. M. Chung, N. F. Ellerton, Viscosity at low shear and circular-dichroism studies of heparin. *Biopolymers* **15**, 1409–1423 (1976).
94. A. Hughes *et al.*, Investigating the relationship between temperature, conformation and calcium binding in heparin model oligosaccharides. *Carbohydr. Res.* **438**, 58–64 (2017).
95. Y. Fang *et al.*, Multiple steps and critical behaviors of the binding of calcium to alginate. *J. Phys. Chem. B* **111**, 2456–2462 (2007).
96. A. J. de Kerchove, M. Elimelech, Formation of polysaccharide gel layers in the presence of Ca2+ and K+ ions: Measurements and mechanisms. *Biomacromolecules* **8**, 113–121 (2007).
97. N. A. Ibrahim, A. A. Nada, B. M. Eid, *Polysaccharide-Based Polymer Gels and Their Potential Applications* (Springer Singapore, 2018), pp. 97-126.
98. A. Assifaoui *et al.*, Structural behaviour differences in low methoxy pectin solutions in the presence of divalent cations (Ca2+ and Zn2+): A process driven by the binding mechanism of the cation with the galacturonate unit. *Soft Matter* **11**, 551–560 (2015).
99. U. T. D. Huynh, A. Lerbret, F. Neiers, O. Chambin, A. Assifaoui, Binding of divalent cations to polygalacturonate: A mechanism driven by the hydration water. *J. Phys. Chem. B* **120**, 1021–1032 (2016).
100. Y. Lei *et al.*, Preparation and property of a biantenna macromolecule based on polysialic acid. *Int. J. Biol. Macromol.* **155**, 1342–1349 (2020).
101. C. M. Runnels *et al.*, Folding, assembly, and persistence: The essential nature and origins of biopolymers. *J. Mol. Evol.* **86**, 598–610 (2018).